# Rapid prediction of breast biomechanics under gravity loading using surrogate machine learning models

**Max Dang Vu[1], Gonzalo D. Maso Talou[1], Huidong Bai[1], Poul M. F. Nielsen[1,2], Martyn P. Nash[1,2], Thiranja Prasad Babarenda Gamage[1]**

[1]Auckland Bioengineering Institute and [2]Department of Engineering Science, University of Auckland, Auckland, New Zealand.

**Abstract** Identifying and localising breast tumours is challenged by differing patient orientation between clinical examination and treatment procedures. Individual-specific, physics-driven models of the breast can help clinicians track and co-locate information between medical images acquired from different modalities but are unsuitable for real-time intervention. We present a surrogate machine learning model that predicts the breast's mechanical behaviour under gravity loading in near real-time. A high-fidelity finite element (FE) model simulating material point displacements $\boldsymbol{d}$ of the breast, using a reference geometry and combinations of a constitutive material parameter $C_1$ and the relative orientation of the breast with respect to gravity $\boldsymbol{g}$, was used to generate synthetic ground truth data. The best-trained surrogate model produced an error of 0.13 mm ± 0.03 mm with respect to the $L_2$-norm of the FE model's displacement field in model validation. This model can predict the material point displacement of the breast in clinically relevant orientations (e.g., prone and supine) with a maximum root mean squared error of 1.04 mm (SD 1.08 mm). The computations took around 2.0 s to 2.1 s, up to 82.5 times faster than the equivalent FE models on a CPU. The proposed approach is therefore promising for developing augmented reality tools to aid with real-time clinical navigation of soft tissues.

## 1 Introduction

Approximately 2.3 million women are diagnosed with breast cancer, and another 685,000 women die from the disease annually [1]. Early detection and surgical removal of tumours help improve patient outcomes [2]. Tumour positions are identified and analysed across medical images acquired from X-ray mammography, magnetic resonance imaging (MRI), and second-look ultrasound (US) (Figure 1). However, patient orientation differs between these imaging modalities and surgery, complicating the matching and localisation of lesions, limiting successful tumour excisions. In such cases, patients must undergo re-operation which ranges from 19 % to 22 % of patients who underwent breast-conserving surgery in New Zealand [3], [4], and across the world [5]–[8]. Re-operation is associated with increased morbidity, treatment duration, cost of care and worsened cosmetic outcomes [5].

a b c

**Fig. 1** Breast cancer diagnostic images acquired using (a) mammography in the standing position, followed by (b) MRI in the prone position and (c) US in the supine-tilted position. Image a (Monkey Business - stock.adobe.com), Image b (siemens.com/press), Image c (Luisandres - stock.adobe.com).

Such clinical challenges have motivated the development of physics-driven computational models to help clinicians accurately track and co-locate lesions during procedures. These models use the finite element method (FEM) to predict breast tissue deformation from prone (orientation in MRI) to supine (orientation in surgery) under gravity loading [9]–[11]. However, this approach is computationally expensive for simulating large nonlinear deformations [12]. State-of-the-art FE breast models take at least 30 seconds to solve [13], which makes clinical translation difficult.

Surrogate machine learning models, commonly referred to as surrogate models, can rapidly mimic the behaviour of FE models and achieve similar accuracy to the FE model [14]. Martinez-Martinez (2017) [15] used a decision tree, extremely randomised trees, and random forest methods to train surrogate models that predict whole breast deformation under compression in less than 0.15 s. Mendizabal (2020) [16] trained models with U-Nets to predict ultrasound-probe-induced displacements of breast tissue lesions in about 3 ms. However, both models were trained offline for specific geometries and loading conditions, hence re-training was required for any changes to the mechanical problem.

We have developed a surrogate modelling framework for cardiac mechanics to avoid the need for re-training [17]. An intrinsic learning domain was created using diffeomorphic mapping to preserve the geometry's topology, ensuring that the surrogate model was application-agnostic. The validated model, trained using Siamese neural networks, took 0.7 s to predict the left ventricular displacement during passive filling (62 times faster than the FE model) and approximately 9 s to estimate one constitutive parameter of the model [18]. This work documents the application of this surrogate modelling framework in rapidly predicting the material point displacement of a personalised biomechanical model of the breast in multiple orientations subject to gravity loading. Note that material point displacement refers to the displacement of nodes in a FE model and their equivalents in the surrogate model.

The manuscript is structured as follows. Section 2 details the development of the surrogate model, and the training and performance evaluation results. Section 3 presents the predicted material displacements, and the model's accuracy and efficiency compared to the equivalent FE model results. Section 4 discusses the

findings and the model's future developments. Section 5 provides concluding remarks.

## 2 Methods

This section presents a sequential modelling framework (see Figure 2) to generate and benchmark surrogate models with a chosen high-fidelity model. In particular, we used a FE model of the breast under gravity loading published elsewhere [11] as the high-fidelity model. This model's predictions demonstrated good agreement (RMS error of 0.64 mm) with the scanned surface of a deformed phantom in experimental validation studies [9], [19].

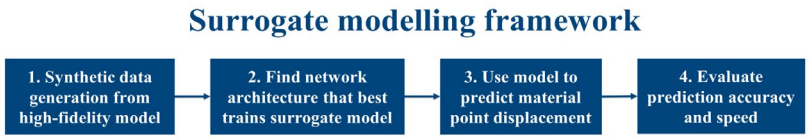


**Fig. 2** The surrogate models are trained using synthetic ground truth data from a FE model that simulates the material point displacement of the breast for a given constitutive material parameter, orientation with respect to gravity, and reference geometry. Several network architectures were used for training, and we selected the network that yielded the surrogate model with the lowest validation error with respect to the $L_2$-norm of the FE model's displacement field. This model's prediction accuracy and time compared to the FE model were evaluated to assess its performance.

Ground truth data for training the surrogate model was obtained from the above FE model implemented in OpenCMISS [21]. An automated imaging analysis workflow [22] used the 1 $mm^3$ T2-weighted MR image of a healthy 49-year-old volunteer, acquired in the prone position at the University of Auckland's Centre for Advanced Magnetic Resonance Imaging (CAMRI), to construct an individual-specific anatomical model of the torso. The breast geometry was segmented from the torso and discretised into a FE mesh for the simulation (Figure 3) [23].

The breast domain was approximated with cubic Lagrange elements, as presented in Figure 3. The FE model assumes that breast tissue is incompressible, isotropic, and homogeneous, and has a material density of 900 $kg{\cdot}m^{-3}$ [9], [19], [20]. The mechanical behaviour of breast tissues was simulated using a neo-Hookean hyperelastic strain energy function $\boldsymbol{W} = C_1\,(\boldsymbol{I_1} - 3)$, where $C_1$ is the constitutive material parameter, and $I_1$ is the first invariant of the right Cauchy-Green deformation tensor [24]. Homogeneous Dirichlet boundary conditions were applied on the outer rib boundary to model the rigid attachment between the breast and the anterior chest wall [25], [26].

Synthetic breast displacement data $\boldsymbol{d} = [dx, dy, dz]$ was generated from the high-fidelity FE model using a reference geometry (with coordinates $x$, $y$, $z$), $C_1$ and relative orientation of the gravity force $\boldsymbol{g} = [g_x, g_y, g_z]$ $m{\cdot}s^{-2}$. The orientation of $\boldsymbol{g}$ is defined in spherical coordinates (Figure 4) (Equation 1). 688 mechanical setups

were evaluated using the FE model, and each sampled 3,545 material points in the domain, yielding a total of 2,438,960 samples for the dataset (Table 1). These samples were partitioned as 80 % for training, 10 % for testing and 10 % for validating the surrogate model.

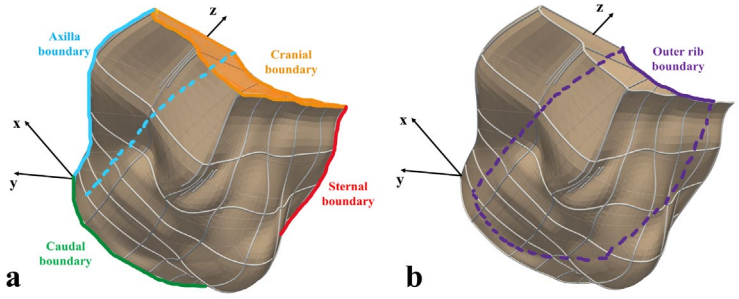


**Fig. 3** a) The breast model was segmented from the anatomical model of a torso, and the cranial, caudal, sternal and axilla surfaces were defined as the model boundaries. b) The breast geometry is the FE domain of interest, and the outer rib boundary is the posterior surface of the breast [23].

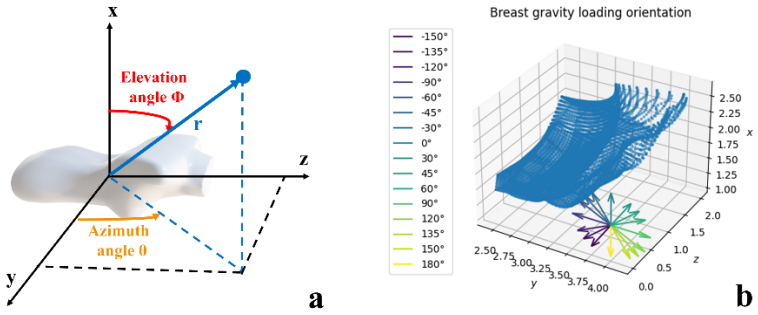


**Fig. 4** a) Orientation of gravity (***g***) with respect to the breast was defined in spherical coordinates, where r is the magnitude (9.81 $m{\cdot}s^{-2}$), $\Phi$ is the elevation angle, and $\theta$ is the azimuth angle. The combination of $\Phi = 0^o$ and $\theta = 0^o$ represents the gravity force orientation for the supine breast, while $\Phi = 180^o$ and $\theta = 0^o$ represent the gravity force orientation for the prone breast. b) The arrows indicate the ***g*** orientation where $\Phi$ varies between -150° and 180°, and $\theta$ was fixed at 0° to simulate the torso rotation about the cranio-caudal (z) axis direction. Note that the breast model point cloud has been downsampled 100 times for illustration purposes in this figure.

$$[g_x, g_y, g_z] = 9.81\,[cos\,\Phi, sin\,\Phi\,cos\,\theta, sin\,\Phi\,sin\,\theta\,] \quad \textbf{(1)}$$

**Table 1.** Sampling of the mechanical parameters used to generate the synthetic dataset.

| Parameter | Step | Range | Samples |
|---|---|---|---|
| $C_1$ (kPa) | 0.1 | [0.8, 5.0] | 43 |
| $\Phi$ (degrees, °) | variable | [-150, 180] | 16 |

The surrogate model was trained using a Siamese neural network [27] and implemented in TensorFlow, an open-source machine learning library [28]. One network trains the domain nodes (non-boundary nodes) to predict the material point displacement, whilst the other trains the boundary nodes to enforce the Dirichlet boundary condition. The network architecture consists of hidden dense layers containing neurons and a single final output layer. All neurons are connected to those on the successive layer to increase the network's capacity. The output layer has three neurons to predict *dx*, *dy* and *dz*, respectively. The error between the ground truth dataset and the surrogate prediction is computed using a loss function that combines the $L^2$ norm error of the domain and boundary networks (Equation 2), where $u$ is the predicted displacement, $\hat{u}$ is the FE model displacement, $B$ is a set of points in the domain or boundary, and the subindexes $b$ and $d$ denote points on the boundary or the domain, respectively. A penalisation factor $\alpha$ applied on the boundary network helps to enforce the boundary conditions. Weights of the trained network are obtained when the loss function is minimised.

$$L = \sum_{u_d \in B_d} \left|\left|u_d - \hat{u}_d\right|\right|_2 + \alpha \sum_{u_b \in B_b} \left|\left|u_b - \hat{u}_b\right|\right|_2 \quad \textbf{(2)}$$

The network was trained using the ADAM algorithm [29] with network weights of 0.5 and 0.9 respectively, a learning rate of 0.01 and a batch size of 8000 samples during 200 epochs at maximum. A patience parameter of 20 stops training when the validation loss function does not improve after 20 epochs. The network was trained with nine different architectures to investigate the sensitivity of training accuracy to network architecture. These networks contain 2, 3, and 4 identical layers with 32, 64, and 128 neurons each. The network architecture with the lowest error during validation (see Equation 2) was selected as the best-trained network for further training of the surrogate model.

The trained and validated surrogate model was used to predict the material point displacement of presented cases. The prediction error was quantified using the root mean squared error (RMS error) (Equation 3) between the FE model results and the surrogate model predictions. Secondly, the prediction speed of the surrogate model was compared against the solution time for the FE model using the average wall clock time, and the distribution of such times over repeated experiments was analysed.

$$\varepsilon = \frac{\sum_{i=1}^{N} \sqrt{(u_{i,x} - \hat{u}_{i,x})^2 + (u_{i,y} - \hat{u}_{i,y})^2 + (u_{i,z} - \hat{u}_{i,z})^2}}{N} \quad \textbf{(3)}$$

# 3 Results

Here, we showcase: (1) the neural network architecture that best trained a surrogate model using synthetic data from the FE model; (2) how accurately this surrogate model predicted the material point displacements compared to the synthetic data; and (3) the relative times taken to perform the task.

The surrogate model was trained using nine different Siamese neural network architectures to find the network that achieved the lowest prediction error (see Table 2). The model was trained five times with each architecture on an NVIDIA Tesla V100 GPU. The mean and standard deviation of validation error was reported, alongside the training time for each architecture. Preliminary findings show that the best–ranked surrogate model was trained with a network architecture of 3 hidden layers and 32 neurons per layer (lowest validation error of 0.13 mm ± 0.03 mm), and model training took approximately 3155 s ± 60 s (between 51 minutes and 54 minutes).

**Table 2.** Prediction errors of surrogate models trained using Siamese neural networks with a varying number of hidden layers and neurons per hidden layer.

| **Architecture (layers x $n_i$)** | **Mean ± SD validation error (mm)** | **Mean ± SD training time (s)** |
|---|---|---|
| 2 x 32 | 0.31 ± 0.06 | 2663 ± 110 |
| 2 x 64 | 0.21 ± 0.06 | 2632 ± 98 |
| 2 x 128 | 0.27 ± 0.10 | 2715 ± 105 |
| **3 x 32** | **0.13 ± 0.03** | **3155 ± 60** |
| 3 x 64 | 1.27 ± 0.26 | 1171 ± 168 |
| 3 x 128 | 1.43 ± 0.60 | 1414 ± 982 |
| 4 x 32 | 1.15 ± 0.56 | 1842 ± 1051 |
| 4 x 64 | 0.92 ± 0.77 | 2420 ± 1175 |
| 4 x 128 | 1.14 ± 0.19 | 1390 ± 164 |

We used the best-trained surrogate model to predict material displacements of the breast for clinically relevant orientations, i.e. gravity force representing the prone and supine orientations. Figure 5 demonstrates the ability of the surrogate model to predict material point displacements for a breast in the prone and supine positions. We used $C_1$ values of 1.0 kPa and 5.0 kPa to demonstrate the model's ability to predict a variety of nonlinear deformation fields, and the associated prediction errors. These predictions are compared quantitatively to the FE model results in Table 3. Compared to the supine orientation, the surrogate model's performance seems to improve with large $C_1$ values and gravity in the prone orientation. The

prediction that incurred the largest possible error (RMS error of 1.04 mm [SD 1.08 mm]) was the 1.0 kPa case with the breast in the supine orientation with respect to the force of gravity.

The FE and surrogate models were executed using an 11th Gen Intel Core i7 CPU at 2.30 GHz. As shown in Table 4, the surrogate models were approximately 70 to 82.5 times faster than the FE framework for simulating breast deformations for the soft models ($C_1$ = 1.0 kPa), and about 37 to 41 times faster for stiff models ($C_1$ = 5.0 kPa).

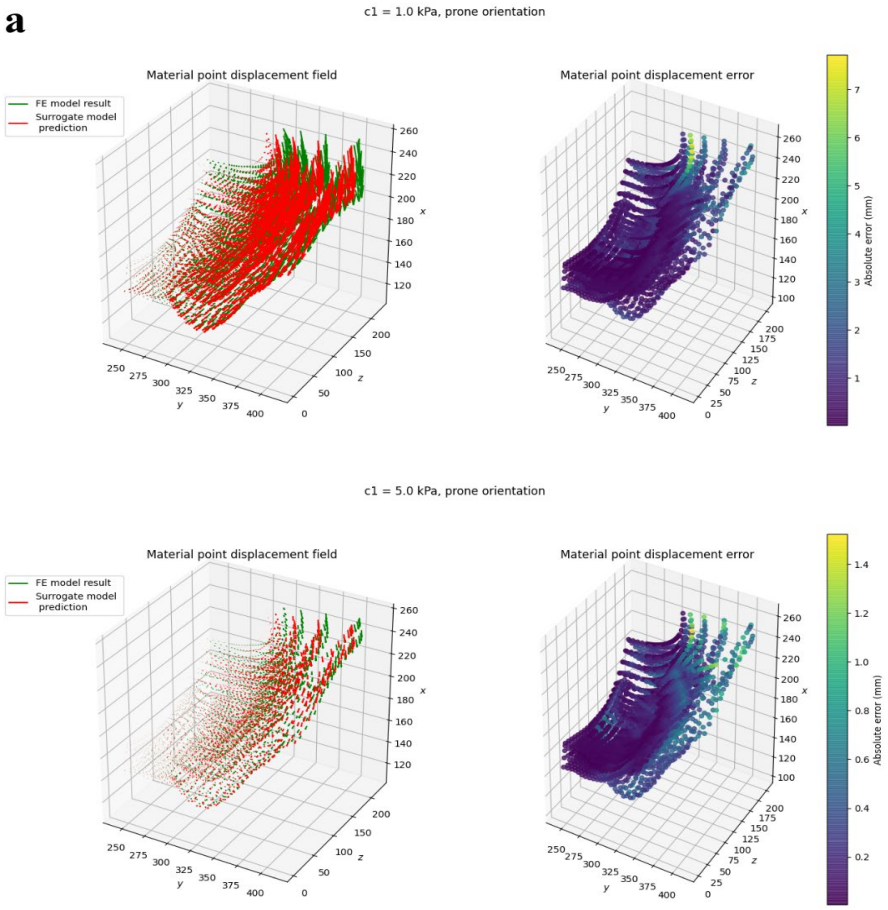

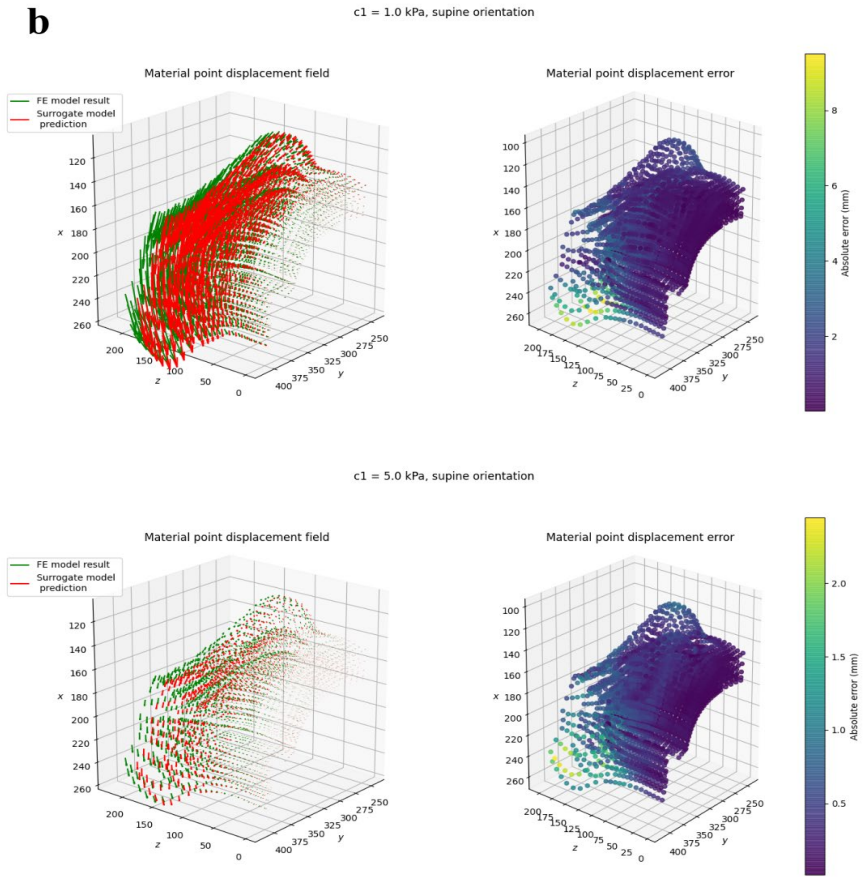


**Fig. 5** Material point displacement field prediction and RMS error with $C_1$ values of 1.0 kPa and 5.0 kPa for breast models in the a) prone and b) supine orientations. The surrogate model's predictions had smaller errors at the outer rib boundaries and the areas surrounding the nipple, and were more prominent for the softer models with $C_1$ = 1.0 kPa. The largest prediction errors were located around the shoulder regions (maximum error of 7.73 mm in the prone orientation for 1.0 kPa. and 9.50 mm in the supine orientation for 1.0 kPa).

**Table 3.** Mean displacements and displacement ranges for the prone and supine gravity-loading orientations computed using FE and surrogate models of the breast. The RMS errors for the surrogate model predictions (compared to the FE models) are also reported to showcase the ranges of errors involved.

| **Model** | **Metrics** | **Prone orientation** | | **Supine orientation** | |
|---|---|---|---|---|---|
| | | **$C_1$ = 1.0 kPa** | **$C_1$= 5.0 kPa** | **$C_1$ = 1.0 kPa** | **$C_1$= 5.0 kPa** |
| FE | Mean displacement (mm) | 3.21 | 0.62 | 3.16 | 0.62 |

| | | | | | |
|---|---|---|---|---|---|
| | Displacement range (mm) | [0, 37.2] | [0, 7.2] | [0, 38.4] | [0, 7.3] |
| Surrogate | Mean displacement (mm) | 3.0 | 0.58 | 2.6 | 0.42 |
| | RMSE ± SD (mm) | 0.70 ± 0.68 | 0.19 ± 0.18 | 1.04 ± 1.08 | 0.30 ± 0.29 |
| | Displacement range (mm) | [0.01, 35.7] | [0.01, 7.3] | [0.00, 36.2] | [0.01, 6.7] |

**Table 4:** Average wall clock time for solving breast models with $C_1$ values of 1.0 kPa and 5.0 kPa in the prone and supine gravity-loaded orientations.

| **Model** | **Prone simulation time (s)** | | **Supine simulation time (s)** | |
|---|---|---|---|---|
| | **$C_1$ = 1.0 kPa** | **$C_1$ = 5.0 kPa** | **$C_1$ = 1.0 kPa** | **$C_1$ = 5.0 kPa** |
| FE | 154 ± 11 | 80.0 ± 1.7 | 152 ± 4 | 82.6 ± 1.6 |
| Surrogate | 2.40 ± 0.02 | 2.36 ± 0.02 | 2.37 ± 0.02 | 2.37 ± 0.02 |

# 4 Discussion

This manuscript presents the development and training of a surrogate model to predict breast tissue displacement under different orientations with respect to gravity. We generated synthetic data using a FE model of the breast implemented in OpenCMISS, and used these data to train, test and evaluate the surrogate modelling approach. We analysed 688 biomechanical FE models of the breast, with different tissue stiffnesses and gravity loading orientations, yielding ~2.4 million samples. We chose $C_1 \in [0.8, 5.0]$ kPa at 0.1 kPa intervals, as the breast model underwent significant deformations for this range of stiffnesses. Gravity force angles $\Phi$ were sampled between -150° and 180° to represent rotations about the cranio-caudal axis, with sample points that were clustered about the poles ($\Phi$ = 0°, 180°) and comparatively sparse about the equator ($\Phi$ = ±90°) of a unit sphere [30] (Figure 4b). Future work could consider setting the probability of placing an arbitrary point proportional to the region's area on the circular cross-section to place more points around the equator [31].

We reported errors observed during validation for surrogate models trained using the nine architectures reported in Maso Talou (2020) [17]. In that case, a 4 x 64 architecture achieved the lowest error (0.044 mm ± 0.029 mm), whereas in the present study, a 3 x 32 architecture performed best (0.13 mm ± 0.03 mm) (Table 2). The use of a wider, deeper network may have led to overtraining of the model, as variations in breast deformations due to variations in gravity loading are generally

less complex than cardiac deformations, and the present study used significantly less training data than the cardiac problem (~ 6 million samples). To confirm this in the future, the training step could be repeated with more data fed to the network to test whether the higher-capacity networks can improve the training performance. We could also increase the number of epochs and the patience parameter to ensure comprehensive model training. An intrinsic breast domain for training has not yet been considered - we could consider using a rectangular domain for the breast topology to check for training performance improvement.

The surrogate model's prediction accuracy was better for the stiffer models (Table 3). The large nonlinear deformations for the soft breast models (maximum of 37.2 mm for $C_1$ of 1.0 kPa) were computationally expensive and challenging to solve using FE modelling. Nevertheless, the surrogate modelling prediction errors were within an average of 1.04 mm (SD 1.08 mm) of the FE model results, which is promising for such large deformations. Similarly to Martinez-Martinez [15], predictions of the proposed model fall within the 5 mm error range accepted clinically, whereas Mendizabal's validation studies on a breast phantom averaged a target registration error of 6.2 mm [16]. The large prediction errors associated with the deformations in the shoulder region near the axilla boundary are a potential concern. Unlike previous works [25], [32], the axilla boundary was not fixed for the simulation as we assumed, for this study, that it does not significantly affect the deformation of the breast region. However, these errors are exaggerated for an extremely low $C_1$ and are less concerning as $C_1$ increases (Figure 5).

The surrogate model was around 70 to 82.5 times faster at computing mechanics of the softer models than the FE model. The speed-up factor reduces to 37 to 41 times for the stiffer models, because surrogate models are agnostic to elastic properties. In contrast, FE models are not (solving FE models with softer properties is generally more computationally intensive). The observed speed-up factors are comparable to [17], which produced surrogate model predictions 62 times faster than equivalent FE models. However, the cardiac model solved within 0.7 s, whereas these breast models took about 2.0 s to 2.1 s. A possible reason for this was that training could be improved by gathering more data or using an intrinsic domain, as discussed earlier. Another contributing factor is that the surrogate cardiac model was executed on a GPU, not on a CPU like the breast model. The proposed surrogate model's speed is slower than similar studies of breast mechanics [15], [16]. However, it was noted that the previous models were designed for different loading conditions, and used different machine learning techniques. To the best of our knowledge, no similar model has been implemented for gravity loading of the breast.

Future aims of this work are to use the proposed surrogate modelling approach to estimate breast tissue constitutive parameters rapidly, and subsequently validate the framework using a silicone gel breast phantom. This will build on related studies for identifying the mechanical properties of soft materials [11], [33], [34]. These steps are essential for the development of a software platform [35] that integrates physics-driven computational modelling with augmented reality technology [36], [37] and state-of-the-art model visualisation techniques [38] to align diagnostic images with 3D holograms of biomechanical models. This platform could

eventually extend our automated clinical image analysis workflow [22] to provide clinicians with real-time navigational guidance during breast cancer imaging and treatment procedures (Figure 6).

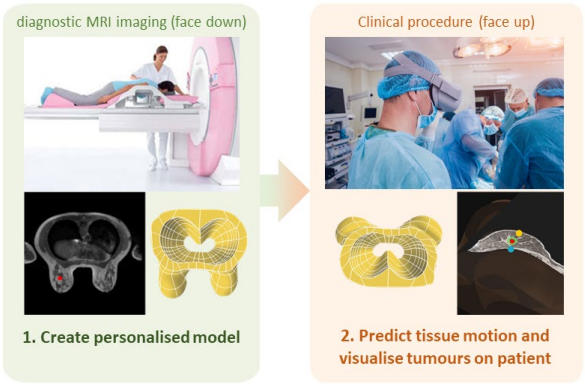


**Fig. 6** A proposed augmented reality platform will leverage an automated clinical workflow for breast cancer image analysis. The workflow builds personalised biomechanical models of the breast from diagnostic MRI and visualises breast tissue displacements in near real-time during clinical procedures performed in the supine position. Some images were obtained from Romaset - stock.adobe.com.

## 5 Conclusion

We presented a surrogate modelling framework that predicts material point displacement of a personalised breast model under gravity loading and varying constitutive material parameters in about 2.0 s to 2.1 s. The surrogate model was trained with 688 FE models representing different biomechanical setups, and achieved errors of 0.13 mm ± 0.03 mm compared to the FE model solutions. Surrogate models predicted the material point displacements about 70 to 82.5 times faster than the state-of-the-art FE model, and the maximum prediction errors averaged at only 1.04 mm (SD 1.08 mm) for soft models of the breast. This suggests that the proposed surrogate model can simulate mechanical deformation very efficiently. It also represents a promising development toward applying real-time, personalised biomechanical modelling to help improve breast cancer diagnosis and treatment practices.

**Acknowledgements** The authors are grateful for financial support from the New Zealand Government's Ministry for Business, Innovation and Employment (UOAX1004), the New Zealand Breast Cancer Foundation (R1704) and the University of Auckland Foundation (F-IBE-BIP). Max Dang Vu is supported by a University of Auckland Doctoral Scholarship. We also thank Mr Stephen Creamer and Mr Chinchien Lin for their valuable contributions to this study.

# References


[1] H. Sung *et al.*, 'Global cancer statistics 2020: GLOBOCAN estimates of incidence and mortality worldwide for 36 cancers in 185 countries', *CA. Cancer J. Clin.*, vol. 71, no. 3, pp. 209–249, 2021, doi: 10.3322/caac.21660.

[2] M. S. Abrahimi, M. Elwood, R. Lawrenson, I. Campbell, and S. Tin Tin, 'Associated factors and survival outcomes for breast conserving surgery versus mastectomy among New Zealand women with early-stage breast cancer', *Int. J. Environ. Res. Public. Health*, vol. 18, no. 5, p. 2738, Mar. 2021, doi: 10.3390/ijerph18052738.

[3] C. Ooi, I. Campbell, J. Kollias, and P. de Silva, 'National breast cancer audit: overview of invasive breast cancer in New Zealand', *N. Z. Med. J. Online*, vol. 125, no. 1359, pp. 7–16, 2012.

[4] A. Gautier, V. Harvey, S. Kleinsman, N. Knowlton, A. Lasham, and R. Ramsaroop, '30,000 voices: informing a better future for breast cancer in Aotearoa New Zealand. Breast Cancer Foundation National Register 2003-2020.' Breast Cancer Foundation NZ, 2022.

[5] F. Tamburelli *et al.*, 'Reoperation rate after breast conserving surgery as quality indicator in breast cancer treatment: A reappraisal', *The Breast*, vol. 53, pp. 181–188, Oct. 2020, doi: 10.1016/j.breast.2020.07.008.

[6] M. T. van Leeuwen *et al.*, 'Reoperation after breast-conserving surgery for cancer in Australia: statewide cohort study of linked hospital data', *BMJ Open*, vol. 8, no. 4, p. e020858, Apr. 2018, doi: 10.1136/bmjopen-2017-020858.

[7] A. J. Isaacs, M. L. Gemignani, A. Pusic, and A. Sedrakyan, 'Association of breast conservation surgery for cancer with 90-day re-operation rates in New York state', *JAMA Surg.*, vol. 151, no. 7, p. 648, Jul. 2016, doi: 10.1001/jamasurg.2015.5535.

[8] R. Jeevan *et al.*, 'Re-operation rates after breast conserving surgery for breast cancer among women in England: retrospective study of hospital episode statistics', *BMJ*, vol. 345, no. jul12 2, pp. e4505–e4505, Jul. 2012, doi: 10.1136/bmj.e4505.

[9] V. Rajagopal, J. H. Chung, D. Bullivant, P. M. F. Nielsen, and M. P. Nash, 'Determining the finite elasticity reference state from a loaded configuration', *Int. J. Numer. Methods Eng.*, vol. 72, no. 12, pp. 1434–1451, 2007, doi: 10.1002/nme.2045.

[10] A. W. C. Lee, 'Breast image fusion using biomechanics', PhD, The University of Auckland, Auckland Bioengineering Institute, 2011.

[11] T. P. Babarenda Gamage, 'Constitutive parameter identifiability and the design of experiments for applications in breast biomechanics', PhD, The University of Auckland, Auckland Bioengineering Institute, 2016.

[12] R. Phellan, B. Hachem, J. Clin, J. M. Mac-Thiong, and L. Duong, 'Real-time biomechanics using the finite element method and machine learning: Review and perspective', *Med. Phys.*, vol. 48, no. 1, pp. 7–18, 2021, doi: 10.1002/mp.14602.

[13] L. Han *et al.*, 'A nonlinear biomechanical model based registration method for aligning prone and supine MR breast images', *IEEE Trans. Med. Imaging*, vol. 33, no. 3, pp. 682–694, 2014, doi: 10.1109/TMI.2013.2294539.

[14] C. Wang, Q. Duan, W. Gong, A. Ye, Z. Di, and C. Miao, 'An evaluation of adaptive surrogate modeling based optimisation with two benchmark problems', *Environ. Model. Softw.*, vol. 60, pp. 167–179, 2014, doi: 10.1016/j.envsoft.2014.05.026.

[15] F. Martínez-Martínez *et al.*, 'A finite element-based machine learning approach for modeling the mechanical behavior of the breast tissues under compression in real-time', *Comput. Biol. Med.*, vol. 90, no. September, pp. 116–124, 2017, doi: 10.1016/j.compbiomed.2017.09.019.

[16] A. Mendizabal, E. Tagliabue, J.-N. Brunet, D. Dall'Alba, P. Fiorini, and S. Cotin, 'Physics-based deep neural network for real-time lesion tracking in ultrasound-guided breast biopsy', *Comput. Biomech. Med.*, pp. 33–45, 2020, doi: 10.1007/978-3-030-42428-2_4.

[17] G. D. Maso Talou, T. P. Babarenda Gamage, M. Sagar, and M. P. Nash, 'Deep learning over reduced intrinsic domains for efficient mechanics of the left ventricle', *Front. Phys.*,

vol. 8, pp. 1–14, 2020, doi: 10.3389/fphy.2020.00030.
[18] G. D. Maso Talou, T. P. Babarenda Gamage, and M. P. Nash, 'Efficient ventricular parameter estimation using AI-surrogate models', *Front. Physiol.*, vol. 12, no. October, pp. 1–14, 2021, doi: 10.3389/fphys.2021.732351.
[19] J. H. Chung, V. Rajagopal, P. M. F. Nielsen, and M. P. Nash, 'A biomechanical model of mammographic compressions', *Biomech. Model. Mechanobiol.*, vol. 7, no. 1, pp. 43–52, Feb. 2008, doi: 10.1007/s10237-006-0074-6.
[20] T. P. Babarenda Gamage, V. Rajagopal, M. Ehrgott, M. P. Nash, and P. M. F. Nielsen, 'Identification of mechanical properties of heterogeneous soft bodies using gravity loading', *Int. J. Numer. Methods Biomed. Eng.*, vol. 27, no. 4, pp. 391–407, 2011, doi: 10.1002/cnm.1429.
[21] C. Bradley *et al.*, 'OpenCMISS: A multi-physics & multi-scale computational infrastructure for the VPH/Physiome project', *Prog. Biophys. Mol. Biol.*, vol. 107, no. 1, pp. 32–47, Oct. 2011, doi: 10.1016/j.pbiomolbio.2011.06.015.
[22] T. P. Babarenda Gamage *et al.*, 'An automated computational biomechanics workflow for improving breast cancer diagnosis and treatment', *Interface Focus*, vol. 9, no. 4, pp. 1–12, 2019, doi: 10.1098/rsfs.2019.0034.
[23] T. P. Babarenda Gamage, H. Y. Baluwala, M. P. Nash, and P. M. F. Nielsen, 'Registration of prone and supine breast MRI for breast cancer treatment planning', in *Computational Biomechanics for Medicine*, A. Wittek, G. Joldes, P. M. F. Nielsen, B. J. Doyle, and K. Miller, Eds. Cham: Springer International Publishing, 2017, pp. 123–134. doi: 10.1007/978-3-319-54481-6_11.
[24] G. A. Holzapfel, *Nonlinear solid mechanics : a continuum approach for engineering*. Chichester ; New York: Wiley, 2000.
[25] T. P. Babarenda Gamage, R. Boyes, V. Rajagopal, P. M. F. Nielsen, and M. P. Nash, 'Modelling prone to supine breast deformation under gravity loading using heterogeneous finite element models', *Comput. Biomech. Med. Deform. Flow*, pp. 29–38, 2012, doi: 10.1007/978-1-4614-3172-5.
[26] D. E. McGhee and J. R. Steele, 'Breast biomechanics: What do we really know?', *Physiology*, vol. 35, no. 2, pp. 144–156, 2020, doi: 10.1152/physiol.00024.2019.
[27] D. Chicco, 'Siamese neural networks: An overview', in *Artificial Neural Networks*, vol. 2190, H. Cartwright, Ed. New York, NY: Springer US, 2021, pp. 73–94. doi: 10.1007/978-1-0716-0826-5_3.
[28] M. Abadi *et al.*, 'TensorFlow: A system for large-scale machine learning', in *12th USENIX Symposium on Operating Systems Design and Implementation (OSDI 16)*, Savannah, GA, Nov. 2016, pp. 265–283. [Online]. Available: https://www.usenix.org/conference/osdi16/technical-sessions/presentation/abadi
[29] D. P. Kingma and J. Lei Ba, 'ADAM: A method for stochastic optimisation', *Int. Conf. Learn. Represent.*, vol. 3rd, pp. 1–15, 2015.
[30] E. W. Weisstein, 'Sphere point picking', *Sphere Point Picking - From MathWorld - A Wolfram Web Resource*, 2002. https://mathworld.wolfram.com/SpherePointPicking.html
[31] M. Deserno, 'How to generate equidistributed points on the surface of a sphere', *Polym. Ed*, vol. 99, no. 2, 2004.
[32] A. W. C. Lee, V. Rajagopal, T. P. Babarenda Gamage, A. J. Doyle, P. M. F. Nielsen, and M. P. Nash, 'Breast lesion co-localisation between X-ray and MR images using finite element modelling', *Med. Image Anal.*, vol. 17, no. 8, pp. 1256–1264, Dec. 2013, doi: 10.1016/j.media.2013.05.011.
[33] V. Rajagopal, 'Modelling breast tissue mechanics under gravity loading', PhD, The University of Auckland, Auckland Bioengineering Institute, 2007.
[34] J.-H. Chung, 'Modelling mammographic mechanics', PhD, The University of Auckland, Auckland Bioengineering Institute, 2008.
[35] M. Dang Vu, 'Pinpointing breast cancer from a bioengineering perspective', *University of Auckland Scientific*, vol. 2, no. 1, pp. 5–8, Mar. 2022.
[36] P. F. Gouveia *et al.*, 'Breast cancer surgery with augmented reality', *Breast*, vol. 56, pp. 14–

17, 2021, doi: 10.1016/j.breast.2021.01.004.
[37] S. L. Perkins, M. A. Lin, S. Srinivasan, A. J. Wheeler, B. A. Hargreaves, and B. L. Daniel, 'A mixed-reality system for breast surgical planning', *Adjun. Proc. 2017 IEEE Int. Symp. Mix. Augment. Real. ISMAR-Adjun. 2017*, pp. 269–274, 2017, doi: 10.1109/ISMAR-Adjunct.2017.92.
[38] R. Laven, 'Markerless tracking of highly deformable objects', Masters, The University of Auckland, Auckland Bioengineering Institute, 2021.